Heating of Mesospheric Air by Sprites and Its Implications for Production of Infrasonic Acoustic Waves

Caitano L. da Silva[1*] and Victor P. Pasko[1]

[1]Communications and Space Sciences Laboratory, Department of Electrical Engineering
Penn State University, University Park, PA, USA

ABSTRACT: Acceleration, expansion, and branching of sprite streamers can lead to concentration of high electrical currents in regions of space, that are observed in the form of bright sprite cores. Driven by this electrical current, a series of chemical processes take place in the sprite plasma. Excitation, followed by quenching of excited electronic states leads to energy transfer from charged to neutral species. The consequence is heating and expansion of air leading to emission of infrasonic acoustic waves. Our results indicate that $\gtrsim$0.01 Pa pressure perturbations on the ground, observed in association with sprites, can only be produced by exceptionally strong currents in sprite cores, exceeding 2 kA.

INTRODUCTION

Sprites are large scale electrical discharges occurring between 40 and 90 km altitude [*Sentman et al.*, 1995]. They are generated by strong quasi-electrostatic fields produced by cloud-to-ground lightning discharges in an underlying thunderstorm. Sprites have been extensively studied through measurements of their optical emissions [e.g., *Stenbaek-Nielsen and McHarg*, 2008] and remote sensing of their electromagnetic fields [e.g., *Cummer et al.*, 1998]. In recent years a new possibility for sprite remote sensing has been realized: infrasound signatures recorded on the ground have been unambiguously associated with sprites [*Farges et al.*, 2005]. The possibility of infrasound generation by sprites was first proposed by *Bedard et al.* [1999]. *Liszka* [2004] reported the detection of infrasound signatures that were associated with sources at mesospheric altitudes during times of intense thunderstorm activity. These findings were confirmed by *Farges et al.* [2005], whose authors have correlated the infrasound recordings (in the frequency range of 0.1–9 Hz) with optical sprite observations. Typical sprite infrasound amplitudes are 0.01–0.1 Pa, as measured on the ground, at distances $\sim$100–400 km from the source [*Farges et al.*, 2005; *Farges and Blanc*, 2010]. Long-range sprite infrasound signatures have a chirp-like feature, with low frequencies arriving at the detector before high frequencies [*Farges et al.*, 2005].

Farges et al. [2005] estimated that energies of the order of $\sim$0.4–40 GJ have to be locally deposited by sprites to generate the observed infrasound amplitudes on the ground, far away from the source. These values for energy deposition are well above the ones estimated from optical emissions, which are on the order of several to tens of MJ [e.g. *Sentman et al.*, 2003; *Kuo et al.*, 2008]. In this paper we describe the mechanism of infrasonic acoustic wave generation by fast air heating in sprite cores, and the relationship between infrasound amplitudes and sprite currents [*da Silva and Pasko*, 2014]. The proposed model is a tool to investigate the above mentioned energy discrepancy on energy deposition estimates.

MODEL FORMULATION

The conceptual model of the sprite infrasonic source is depicted in Figure 1a. Sprites manifest themselves in the form of streamer discharges or, more precisely, streamer coronas. Typically, a sprite is initiated from a local inhomogeneity present in the lower ionospheric conductivity, developing as an initial downward positive streamer that accelerates, expands and branches [e.g., *Liu et al.*, 2009]. In some sprites, the

*Corresponding author email: caitano.dasilva@psu.edu, Postal address: 227 Electrical Engineering East, University Park, PA 16802, USA.

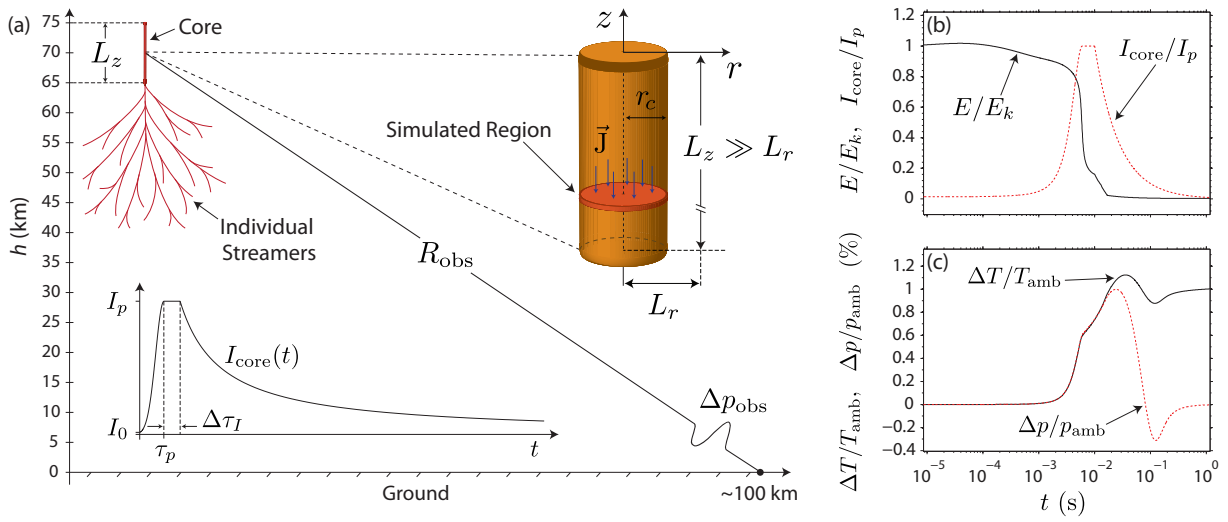

Figure 1: (a) Schematics of air heating in a sprite core leading to generation of infrasonic acoustic waves observed on the ground, at a distance $R_{\rm obs}$ from the source. The figure highlights the geometry of the simulated region, which describes a cross section of the sprite core at $h = 70$ km altitude. The inset shows the waveform of the current flowing through the sprite core, $I_{\rm core}(t)$. (b,c) Time dynamics of electric field and current (b), and maximum modification in temperature and pressure (c) [*da Silva and Pasko*, 2014, Fig. 1]. Reprinted by permission from American Geophysical Union.

development of downward streamers is followed by the formation of upward streamers, depending on the available lightning electric field [*Qin et al.*, 2013]. Sprites with only downward streamers are referred to as column sprites, while those with both downward and upward streamers are referred to as carrot sprites. A common characteristic for both types of morphologies is the existence of a bright core associated with the path traced by the first downward streamer. The schematics of a sprite core, shown in Figure 1, is consistent with sprite morphology observed at submillisecond time resolution [*Cummer et al.*, 2006]. We associate the strong brightness of the sprite core, as evidenced in high speed imagery [e.g., *Cummer et al.*, 2006; *Stenbaek-Nielsen and McHarg*, 2008], with the passage of a strong current through it. This mechanism is different from the one associated with processes in the sprite streamer heads, where very bright and compact regions are formed due to the existence of strong space charge fields of $\sim$3–5E_k [e.g., *Liu et al.*, 2009] (where E_k is the breakdown threshold field defined by the equality between ionization and two-body attachment frequencies in air [e.g., *Raizer*, 1991, p. 135]). As inferred from optical observations [e.g., *Cummer et al.*, 2006], the sprite core has a length $L_z \simeq 10$ km. On the other hand, the transverse scale L_r, is of the order of tens to hundreds of meters. Since $L_z \gg L_r$, we represent the sprite core by a 1–D axisymmetric radial system, located at an altitude $h = 70$ km, as schematically shown in Figure 1a.

In this conceptual model the sprite current $I_{\rm sprite}$, as inferred from remote sensing of electromagnetic fields [e.g., *Cummer et al.*, 1998], is not flowing in the whole cross sectional area of a sprite ($\sim$1000 km^2), but it is rather confined within the several sprite cores, which have substantially higher conductivity than the regions of the atmosphere in their vicinity. The number of sprite cores $N_{\rm core}$ can vary from event to event, typically from a few to tens of cores and, for quantitative analysis conducted in this paper, we assume that on average a sprite has $N_{\rm core} = 10$. The current flowing through a given sprite core, therefore,

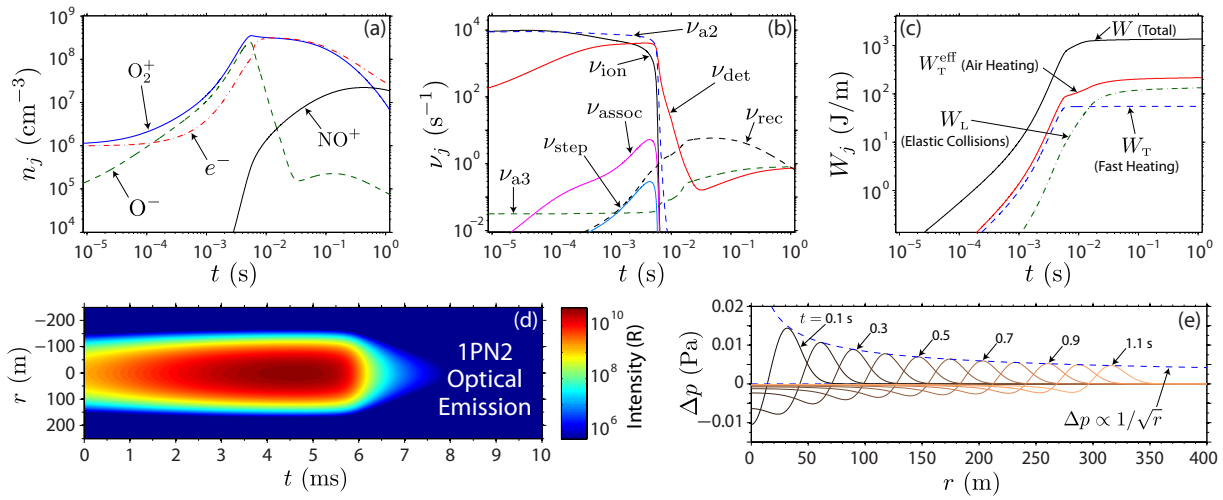

Figure 2: (a,b) Time dynamics (at the axis of symmetry) of main charged species (a), and effective frequencies of electron production and loss (b). (c) Energy deposited per unit channel length. (d) Optical emissions. (e) Radial expansion of pressure wave [*da Silva and Pasko*, 2014, Fig. 2]. Reprinted by permission from American Geophysical Union.

is $I_{\rm core} = I_{\rm sprite}/N_{\rm core}$. The inset in Figure 1a shows the $I_{\rm core}(t)$ waveform adopted in our simulations. The waveform is characterized by three parameters: the peak current I_p, the rise time τ_p (to rise the current from the initial value I_0 to its peak I_p), and the duration of the strong current phase $\Delta\tau_I$. For $t > \tau_p + \Delta\tau_I$ the current slowly decreases as $\propto 1/t$ [e.g., *Barrington-Leigh et al.*, 2002]. The maximum current flowing through a sprite can be estimated from a moving-capacitor plate model [e.g., *Pasko et al.*, 1998; *Barrington-Leigh et al.*, 2002] as being $\sim I_Q h_Q/h_{\rm I}$, where I_Q is the current of the parent cloud-to-ground lightning, h_Q is the altitude of charge removal from the thundercloud, and $h_{\rm I}$ is the lower ionospheric altitude, or the altitude of the moving capacitor plate. For a lightning with high peak current $\sim$100 kA, and $h_Q/h_{\rm I} \simeq 1/5$ (e.g., h_Q =10 km and $h_{\rm I}$ =50 km), one gets $I_{\rm sprite} \leq 20$ kA. We note that, although rare, sprite currents of $\sim$20 kA were already observed [e.g., *Hager et al.*, 2012]. Complementarily, *Cummer et al.* [1998] measured peak currents $I_{\rm sprite} \simeq 2$ kA. Therefore, we estimate that realistic peak currents I_p in bright sprite cores should range between 200 and 2000 A. The time scales τ_p and $\Delta\tau_I$ are adjusted to make the waveform shown in Figure 1a resemble the measurements.

To describe the physical/chemical processes in the sprite core plasma, we have developed a model consisting of four main blocks: (1) a set of non-linear neutral gas dynamics equations; (2) a detailed kinetic scheme accounting for the most important processes in a gas discharge plasma; (3) energy exchange between charged and neutral particles accounting for the partitioning of the electronic power between elastic collisions, excitation of vibrations and excitation of electronic states; and (4) delayed vibrational energy relaxation of nitrogen molecules [*da Silva and Pasko*, 2013a]. This model has also been applied to simulation of leader speeds at reduced air densities and for interpretation of the phenomenology of gigantic jets [*da Silva and Pasko*, 2013b]. An important feature of this model is the capability of calculating the fraction of discharge power σE^2 (where σ is electrical conductivity and E electric field) that is directly used for heating of air in the so called "fast heating" mechanism [e.g., *Popov*, 2011] and its dependence on ambient air density $N_{\rm amb}$. The fast heating mechanism accounts for quenching of excited electronics states, electron

impact dissociation, and electron-ion recombination [*da Silva and Pasko*, 2013a, Sections 2.3 and 3.2].

The initial conditions for the simulation are set to make the sprite core resemble a single sprite streamer channel at 70 km altitude (right after the passage of the first streamer head), i.e., the electron density has a Gaussian radial distribution $n_e = n_{e,a} e^{-r^2/r_c^2}$, where $n_{e,a} = 10^6$ cm^{-3} and $r_c = 20$ m. The value $n_{e,a}$ is the typical electron density in a streamer body as obtained from sprite streamer simulations [e.g., *Liu et al.*, 2009], while r_c is consistent with high-speed optical observations of initial sprite streamer radii [*Kanmae et al.*, 2012]. The choice for r_c is also consistent with observed acoustic spectral content, i.e., a cylindrical acoustic radiator with a diameter of 40 m is expected to produce dominant frequencies below $c_s/2r_c \simeq 8$ Hz, where c_s is the ambient speed of sound. The initial condition for the electric current is $I_0 = q_e(\mu_e + \mu_p) n_{e,a} E_k \pi r_c^2 \simeq 26$ A, where q_e is the electronic charge, and μ_e and μ_p are the mobilities of electrons and positive ions, respectively. The ambient temperature and pressure at 70 km altitude are $T_{\rm amb} = 200$ K and $p_{\rm amb} = 4.68$ Pa, respectively. We apply the current $I_{\rm core}$ to the cross sectional area of the sprite core and we track the plasma parameters, i.e., densities of charged and neutral particles, electric field, translational and vibrational temperature of neutrals, air pressure, etc., as a function of time t, and radial position r, in a cylindrical domain of size $L_r = 400$ m.

RESULTS

The input parameter of the model is the current flowing in the sprite core $I_{\rm core}$. To illustrate the mechanism of infrasonic acoustic wave generation in the sprite core by fast air heating, we discuss in this paper a reference case. We chose a peak current $I_p = 2000$ A in the upper range of sprite core currents (discussed in the previous section), to emphasize that only extraordinary sprites can produce infrasound signatures detectable on the ground. The other parameters of the current waveform are $\tau_p = 6$ ms and $\Delta\tau_I = 4$ ms. Results are shown in Figures 1b–1c and 2a–2e. Figure 1b shows the applied current and the calculated electric field from Ohm's law, it can be seen that an electric field plateau of $\sim E_k$ is sustained during the current growth phase. Figure 1c shows the percent change in temperature and pressure at the axis of symmetry of the sprite core. It can be seen that the maximum modification in pressure is $\sim$1 % and that the highest rate of pressure growth occurs during the current rise stage. Figures 2b–2c show the time dynamics of main charged species and effective frequencies of electron production and loss, following nomenclature used by *da Silva and Pasko* [2013a, Section 2.2 and Table A.1]. Ohm's law indicates that the increase in current should drive an increase in the electric field, however, an incremental increase in the electric field above E_k leads to increase in ionization ($\nu_{\rm ion}$) that leads to conductivity enhancement and reduction of the electric field. Hence, the above mentioned plateau $E \approx E_k$ is formed. In these conditions two-body attachment ($\nu_{\rm a2}$) and ionization rates balance each other. Figures 2b–2c show that the resulting increase in electron density in the sprite core is resulting from the accumulation of O^- ions followed by electron detachment ($\nu_{\rm det}$), in agreement with conclusions of more detailed kinetic models [*Gordillo-Vazquez and Luque*, 2010]. On longer time scales ($t \gtrsim 1$ s) the plasma decays owing to electron-ion recombination ($\nu_{\rm rec}$) and three-body attachment ($\nu_{\rm a3}$).

Figure 2c shows the energy deposited in the sprite core per unit of channel length $W(t)$ (which is obtained by integrating σE^2 over the cross sectional area of the sprite core and in time, i.e., $W(t) = \int_0^t IE(t')dt'$). Total energy deposited per unit channel length is $W = 1.37$ kJ/m (see Figure 2c at the end of the simulation, i.e., $t \simeq 1$ s), which translates in a total energy deposited in the sprite $N_{\rm core} L_z W = 137$ MJ. Figure 2c also shows the calculated amount of energy transferred to heating of air $W_{\rm T}^{\rm eff}(t)$, including fast heating, elastic collisions, heating from ion current, and vibrational-translational energy relaxation ($W_{\rm T}^{\rm eff}$ is obtained by integration of the effective heating rate $Q_{\rm T}^{\rm eff}$, following nomenclature used by *da Silva and Pasko* [2013a, Section 2.3]). A total amount $W_{\rm T}^{\rm eff} = 217$ J/m is used for heating of air, which corresponds to only $\sim$16 % of the total deposited energy. The two major channels for heating of air $W_{\rm T}^{\rm eff}$ are also shown in Figure 2c. During the current rise stage the fast heating mechanism, $W_{\rm T}(t)$, is dominant. During latter stages,

when electric field is signficantly below E_k, $W_{\rm L}(t)$ is dominant; $W_{\rm L}$ accounts for energy transfer in elastic collisions, as well as, excitation of rotations in O_2 and N_2, and vibrations in O_2. Comparing Figures 1b, 1c, and 2c, we can assert that the dominant contribution for pressure increase comes from the fast heating $W_{\rm T}$, during the current rise stage. Moreover, calculation of optical emissions from the sprite core shows that the current rise is also associated with the maximum brightness of the sprite, as shown in Figure 2d. The sustained luminosity associated to rapid current growth is in agreement with the mechanism for the sprite streamer luminous trail proposed by *Liu* [2010]. The direct correlation between current waveform and sprite brightness is also evident in measurements [e.g., *Cummer et al.*, 1998, Figs. 4–6].

Figure 2e shows the radial expansion of the pressure pulse. It can be seen that the response of the neutral gas to this weak source is approximately linear, i.e., pressure amplitudes decrease with distance as $\Delta p \propto 1/\sqrt{r}$, as highlighted by the dashed line in Figure 2e. The maximum pressure amplitude at a reference point $r_{\rm ref} = 10\, r_c$ is $\Delta p_{\rm ref} = 6\times10^{-3}$ Pa. We next estimate the infrasound amplitudes $\Delta p_{\rm obs}$ as measured by an observer on the ground far away from the source, from simple scaling derived from energy conservation. It can be demonstrated that the intensity of an acoustic wave $\mathcal{I}_s$ (expressed in units of J/m^2·s) is related to the amplitude of pressure perturbation as $\mathcal{I}_s = (\Delta p)^2/2\rho_{\rm amb}c_s$ [e.g., *Blackstock*, 2000, pp. 48–51], where $\rho_{\rm amb} = m_{\rm air}N_{\rm amb}$ is the ambient air mass density. Neglecting the effects of atmospheric absorption, the power generated by the source is conserved after the wave has propagated for a distance r, i.e., $\int_S \mathcal{I}_s dS = $ const, where the energy flux is integrated through a reference surface S surrounding the source. The area of this surface is $2\pi r L_z$ and $4\pi r^2$, for a long (cylindrical) radiator and for a (spherical) point source, respectively. Hence, the scaling of the pressure amplitudes with distance and altitude are approximately $\propto\sqrt{N_{\rm amb}}/\sqrt{r}$ and $\propto\sqrt{N_{\rm amb}}/r$, for cylindrical and spherical sources, respectively. Assuming that for sprites the cylindrical dependence holds for a distance about the vertical size of the acoustic radiator (i.e., L_z), we obtain:

$$\Delta p_{\rm obs} = \Delta p_{\rm ref}\sqrt{\frac{N_0}{N_{\rm amb}}}\sqrt{\frac{r_{\rm ref}}{L_z}}\left(\frac{L_z}{R_{\rm obs}}\right), \tag{1}$$

where N_0 and $N_{\rm amb}$ are the ambient air densities at ground level and 70 km altitude, respectively. Assuming that the observation point is at a distance $R_{\rm obs} = 100$ km from the source, as schematically shown in Figure 1a, and for the above defined length scales, this approach gives a correcting factor $\Delta p_{\rm obs}/\Delta p_{\rm ref} \simeq 1.72$, to estimate amplitudes on the ground from amplitudes at a reference position near the source. For the reference case, shown in Figures 1b–1c and 2a–2e, we have $\Delta p_{\rm obs} = 0.01$ Pa, which is in the lower range of amplitudes reported in literature [*Farges et al.*, 2005; *Farges and Blanc*, 2010].

SUMMARY

In this paper we present the mechanism of infrasonic acoustic wave generation by fast air heating in sprite cores. Our results [*da Silva and Pasko*, 2014] demonstrate that $\gtrsim$0.01 Pa pressure perturbations on the ground, observed in association with sprites, can only be produced by exceptionally strong currents in sprite cores, exceeding 2 kA.

ACKNOWLEDGMENTS: This research was supported by NSF AGS-0734083 and AGS-1332199 grants to Penn State University.

References

Barrington-Leigh, C. P., V. P. Pasko, and U. S. Inan (2002), Exponential relaxation of optical emissions in sprites, *J. Geophys. Res.*, *107*(A5), doi:10.1029/2001JA900117.

Bedard, A. J., W. A. Lyons, R. A. Armstrong, B. Hill, and S. Gallagher (1999), A search for low-frequency atmospheric acoustic waves associated with sprites, blue jets, elves, and storm electrical activity, *EOS Trans. Am. Geophys. Union*, *80*(46), Fall Meet. Suppl., Abstract A51B–18.

Blackstock, D. T. (2000), *Fundamentals of Physical Acoustics*, 541 pp., John Wiley & Sons, Inc., New York.

Cummer, S. A., U. S. Inan, T. F. Bell, and C. P. Barrington-Leigh (1998), ELF radiation produced by electrical currents in sprites, *Geophys. Res. Lett.*, *25*(8), 1281–1284, doi:10.1029/98GL50937.

Cummer, S. A., N. C. Jaugey, J. B. Li, W. A. Lyons, T. E. Nelson, and E. A. Gerken (2006), Submillisecond imaging of sprite development and structure, *Geophys. Res. Lett.*, *33*, L04104, doi:10.1029/2005GL024969.

da Silva, C. L., and V. P. Pasko (2013a), Dynamics of streamer-to-leader transition at reduced air densities and its implications for propagation of lightning leaders and gigantic jets, *J. Geophys. Res.*, *118*(24), 13,561–13,590, doi:10.1002/2013JD020618.

da Silva, C. L., and V. P. Pasko (2013b), Vertical structuring of gigantic jets, *Geophys. Res. Lett.*, *40*(12), 3315–3319, doi:10.1002/grl.50596.

da Silva, C. L., and V. P. Pasko (2014), Infrasonic acoustic waves generated by fast air heating in sprite cores, *Geophys. Res. Lett.*, *41*(5), 1789–1795, doi:10.1002/2013GL059164.

Farges, T., and E. Blanc (2010), Characteristics of infrasound from lightning and sprites near thunderstorm areas, *J. Geophys. Res.*, *115*, A00E31, doi:10.1029/2009JA014700.

Farges, T., E. Blanc, A. L. Pichon, T. Neubert, and T. H. Allin (2005), Identification of infrasound produced by sprites during the Sprite2003 campaign, *Geophys. Res. Lett.*, *32*, L01813, doi:10.1029/2004GL021212.

Gordillo-Vazquez, F. J., and A. Luque (2010), Electrical conductivity in sprite streamer channels, *Geophys. Res. Lett.*, *37*, L16809, doi:10.1029/2010GL044349.

Hager, W. W., R. G. Sonnenfeld, W. Feng, T. Kanmae, H. C. Stenbaek-Nielsen, M. G. McHarg, R. K. Haaland, S. A. Cummer, G. Lu, and J. L. Lapierre (2012), Charge rearrangement by sprites over a north Texas mesoscale convective system, *J. Geophys. Res.*, *117*, D22101, doi:10.1029/2012JD018309.

Kanmae, T., H. C. Stenbaek-Nielsen, M. G. McHarg, and R. K. Haaland (2012), Diameter-speed relation of sprite streamers, *J. Phys. D Appl. Phys.*, *45*, 275203, doi:10.1088/0022-3727/45/27/275203.

Kuo, C. L., A. B. Chen, J. K. Chou, L. Y. Tsai, R. R. Hsu, H. T. Su, H. U. Frey, S. B. Mende, Y. Takahashi, and L. C. Lee (2008), Radiative emission and energy deposition in transient luminous events, *J. Phys. D Appl. Phys.*, *41*, 234014, doi:10.1088/0022-3727/41/23/234014.

Liszka, L. (2004), On the possible infrasound generation by sprites, *J. Low Freq. Noise Vib. Act. Control*, *23*(2), 85–93, doi:10.1260/0263092042869838.

Liu, N. (2010), Model of sprite luminous trail caused by increasing streamer current, *Geophys. Res. Lett.*, *37*, L04102, doi:10.1029/2009GL042214.

Liu, N. Y., V. P. Pasko, K. Adams, H. C. Stenbaek-Nielsen, and M. G. McHarg (2009), Comparison of acceleration, expansion, and brightness of sprite streamers obtained from modeling and high-speed video observations, *J. Geophys. Res.*, *114*, A00E03, doi:10.1029/2008JA013720.

Pasko, V. P., U. S. Inan, T. F. Bell, and S. C. Reising (1998), Mechanism of ELF radiation from sprites, *Geophys. Res. Lett.*, *25*(18), 3493–3496, doi:10.1029/98GL02631.

Popov, N. A. (2011), Fast gas heating in a nitrogen-oxygen discharge plasma: I. Kinetic mechanism, *J. Phys. D Appl. Phys.*, *44*, 285201, doi:10.1088/0022-3727/44/28/285201.

Qin, J., S. Celestin, V. P. Pasko, S. A. Cummer, M. G. McHarg, and H. C. Stenbaek-Nielsen (2013), Mechanism of column and carrot sprites derived from optical and radio observations, *Geophys. Res. Lett.*, *40*(17), 4777–4782, doi:10.1002/GRL.50910.

Raizer, Y. P. (1991), *Gas discharge physics*, Springer-Verlag, New York.

Sentman, D. D., E. M. Wescott, D. L. Osborne, D. L. Hampton, and M. J. Heavner (1995), Preliminary results from the Sprites94 aircraft campaign: 1. Red sprites, *Geophys. Res. Lett.*, *22*(10), 1205–1208, doi:10.1029/95GL00583.

Sentman, D. D., E. M. Wescott, R. H. Picard, J. R. Winick, H. C. Stenbaek-Nielsen, E. M. Dewan, D. R. Moudry, F. T. São Sabbas, M. J. Heavner, and J. Morrill (2003), Simultaneous observations of mesospheric gravity waves and sprites generated by a midwestern thunderstorm, *J. Atmos. Solar-Terr. Phys.*, *65*(5), 537–550, doi:10.1016/S1364-6826(02)00328-0.

Stenbaek-Nielsen, H. C., and M. G. McHarg (2008), High time-resolution sprite imaging: observations and implications, *J. Phys. D: Appl. Phys.*, *41*, 234009, doi:10.1088/0022-3727/41/23/234009.